Supporting Information

Core-shell structure of Cu_2O constructed by carbon quantum dots as high performance zinc-ion battery cathode

Qu Zhang [a], Penggao Liu [a], Tao Wang [a, b], Qian Liu [a], and Dongling Wu [a, *]

[a] State Key Laboratory of Chemistry and Utilization of Carbon based Energy Resources; College of Chemistry, Xinjiang University, Urumqi, 830017, Xinjiang, PR China.

[b] Physics and Chemistry Analysis Center, Xinjiang University, Urumqi 830017, China.

[*] Corresponding author.

Tel. +86 09918583083.

E-mail: wudl@xju.edu.cn

Experimental details

Materials: Analytical grade chemicals of, copper sulfate pentahydrate ($CuSO_4 \cdot 5H_2O$), sodium hydroxide (NaOH), trisodium citrate, L-ascorbic acid, hydrogen peroxide solution (30 wt.%) and hydrogen peroxide (H_2O_2, 30%) were purchased from Aladdin Industrial Co., Ltd. (Shanghai) and used without further purification.

Characterization: The morphology was characterized by scanning electron microscopy (SEM, SU8010) and transmission electron microscopy (TEM and HRTEM, JEM-2100). The particle size of all samples was examined by Laser Particle Size Analyzer (S90, Malven). The UV absorption wavelength of CDs was analyzed by UV-Visible Spectrophotometer (UV-3600, Shimadzu). The phase analysis was performed by the Bruker D8 X-ray diffractometer (XRD) with Cu Kα (λ = 1.5418 Å) radiation. Raman spectrum was recorded by using R200-L Raman spectrometer (Bruker) with 532 nm laser. The in-situ Raman spectra were captured from the CV test at 0.6 mV s^{-1} and collected every 90 seconds. Reflectance fourier transform infrared (FTIR) spectra were acquired using a Bruker INVENIO FTIR spectrometer (Karlsruhe, Germany). The surface element state and chemical composition of the samples was analyzed by X-ray photoelectron spectroscopy (XPS, Thermo Fisher, ESCALab250Xi) with Al Kα radiation.

Electrochemical and photoelectrochemical measurements: The slurry mixed with 10 wt.% Ketjen black, 10 wt.% PTFE and 80 wt.% of active material were uniformly coated on a stainless steel mesh and dried at 70 °C for 12 h to obtain Cu_2O-

CDs-X electrodes for electrochemical measurements. The mass loading of active material was 1.1 mg cm^{-2}. The battery was assembled using the Cu_2O-CDs-X electrode as the cathode, zinc metal foil as the negative electrode, a glass fiber as separator, and aqueous 2 M $ZnSO_4$ as electrolyte. The voltage of electrochemical measurement was controlled between 0.2 and 1.1 V. The galvanostatic charge/discharge (GCD) and galvanostatic intermittent titration technique (GITT) tests were performed on the LAND battery test system (CT2001A). The cyclic voltammetry (CV) (voltage was controlled between 0.2 and 1.2 V) and the electrochemical impedance spectroscopy (EIS) tests were recorded on a CHI760E workstation.

Theoretical calculation: All density functional theory (DFT) calculations were performed using the Vienna Ab initio Simulation Package (VASP). The elemental core and valence electrons were represented by the projector augmented wave (PAW) method and plane-wave basis functions with a cut off energy of 550 eV. Generalized gradient approximation with the Perdew-Burke-Ernzerh of GGA-PBE) exchange-correlation functional was employed in all the calculations. Geometry optimizations were performed with the force convergency smaller than 0.05 eV/Å. The DFT-D3 empirical correction method was employed to describe van der Waals interactions. Monkhorst-Pack k-points of 2 × 2 × 1 was applied for all the calculations. A climbing image nudgedelastic band (CI-NEB) method was used to locate the transition states with the same convergence standard.

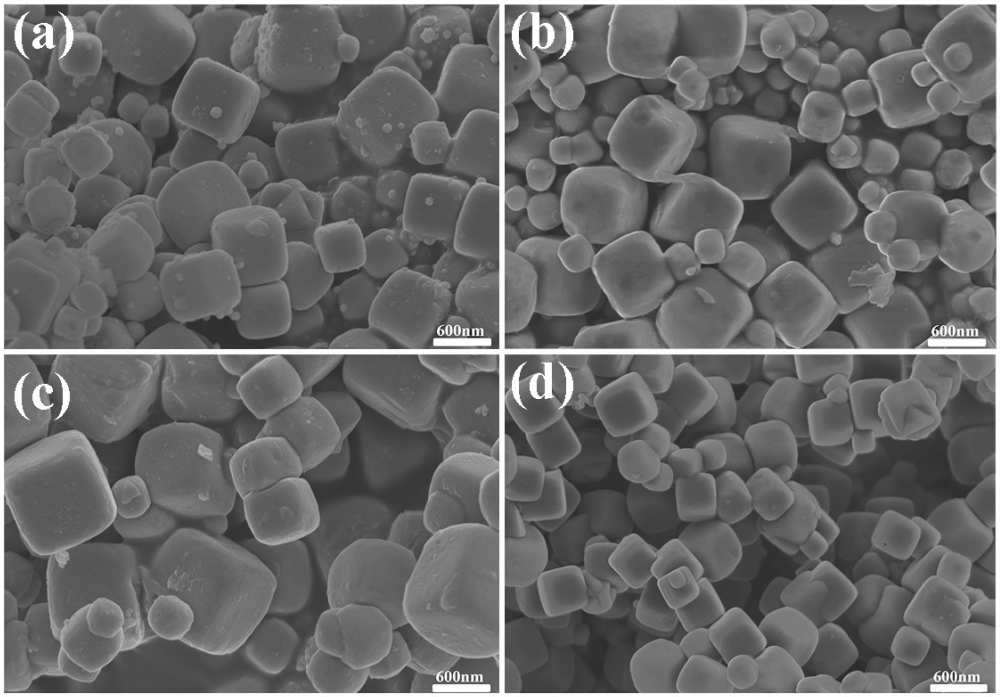

Figure S1. SEM images of (a) Cu_2O-CDs-10, (b) Cu_2O-CDs-20, (c) Cu_2O-CDs-30 and (d) pure Cu_2O.

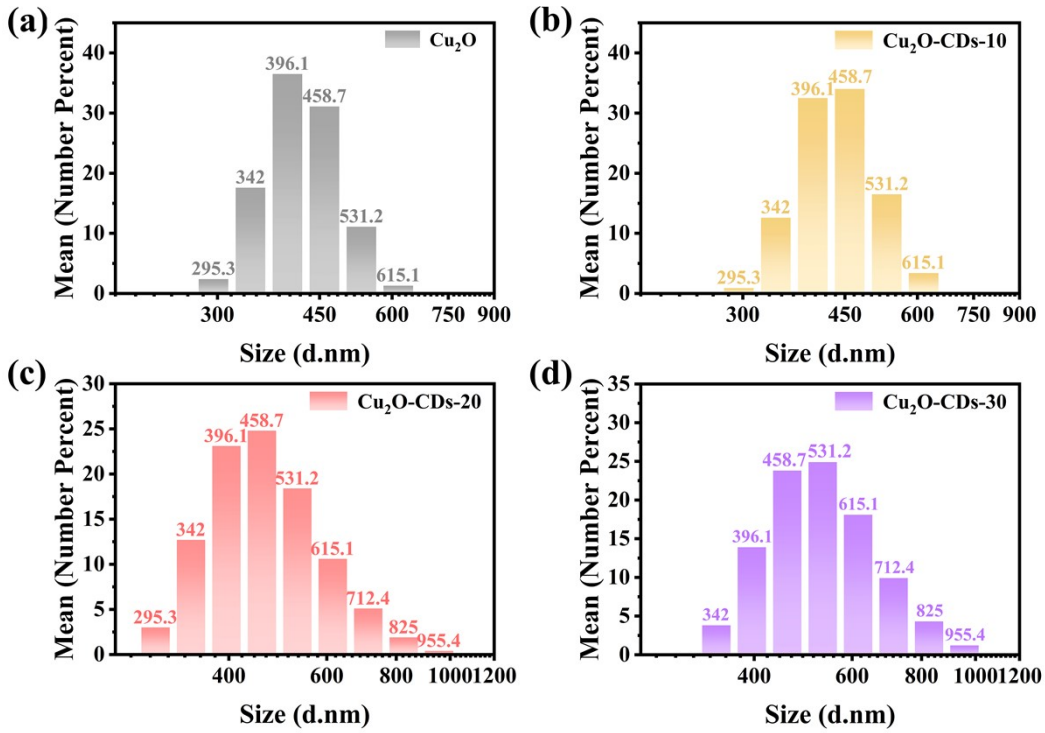

Figure S2. Size distribution of (a) pure Cu_2O, (b) Cu_2O-CDs-10, (c) Cu_2O-CDs-20 and (d) Cu_2O-CDs-30.

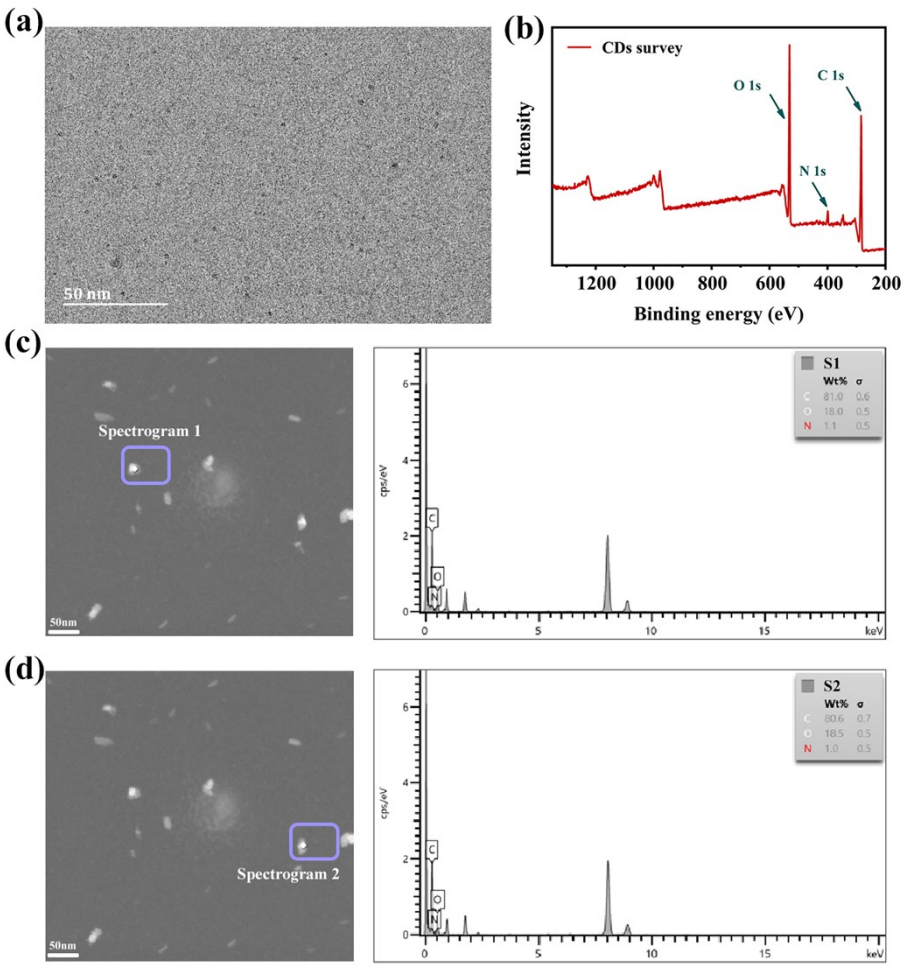

Figure S3. (a) TEM images, (b) XPS-survey, (c) and (d) TEM-EDS of CDs.

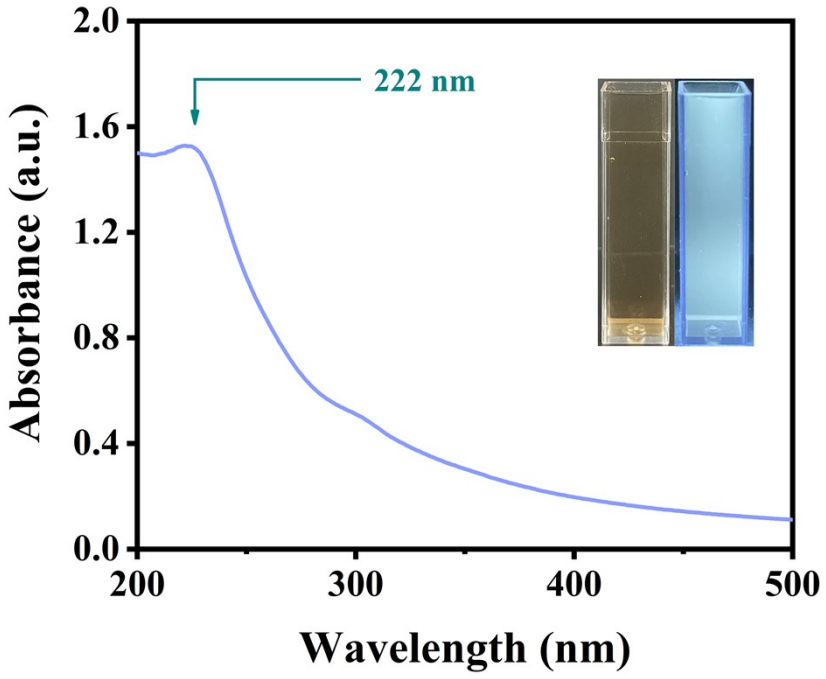

Figure S4. UV-vis spectra of the CDs.

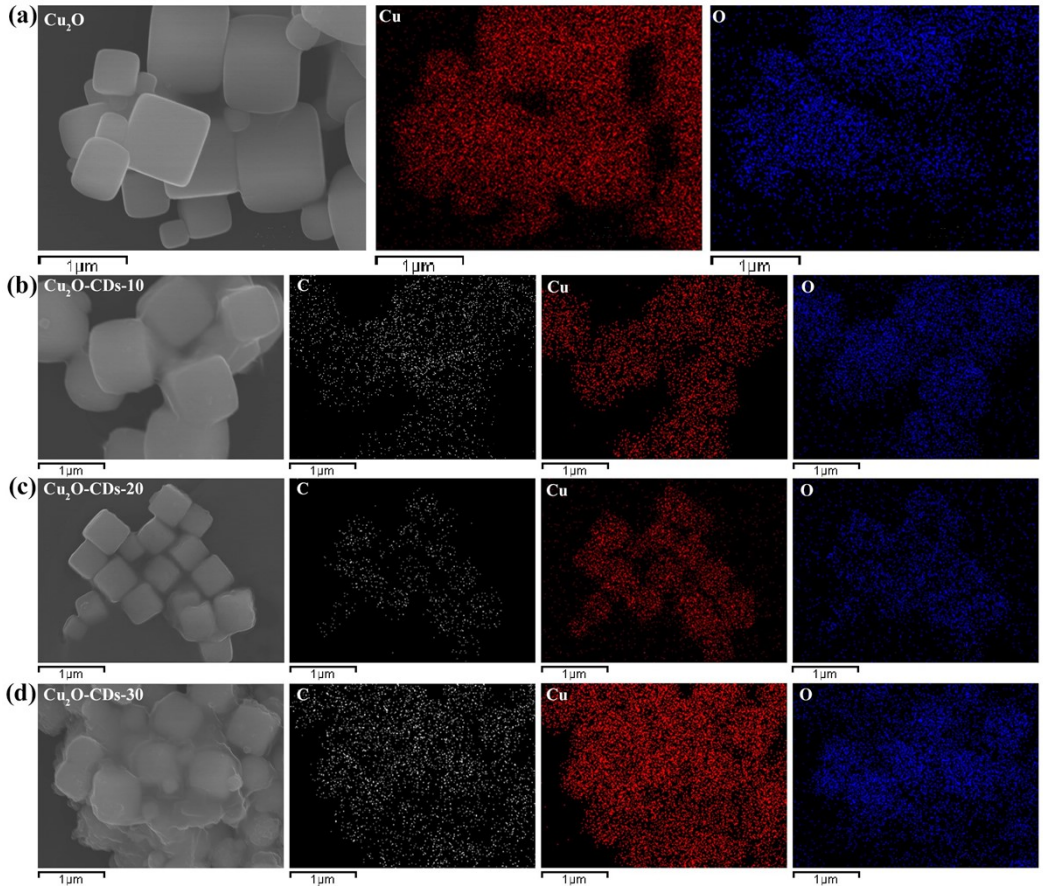

Figure S5. SEM-Mapping of (a) Cu_2O, (b) Cu_2O-CDs-10, (c) Cu_2O-CDs-20 and (d) Cu_2O-CDs-30.

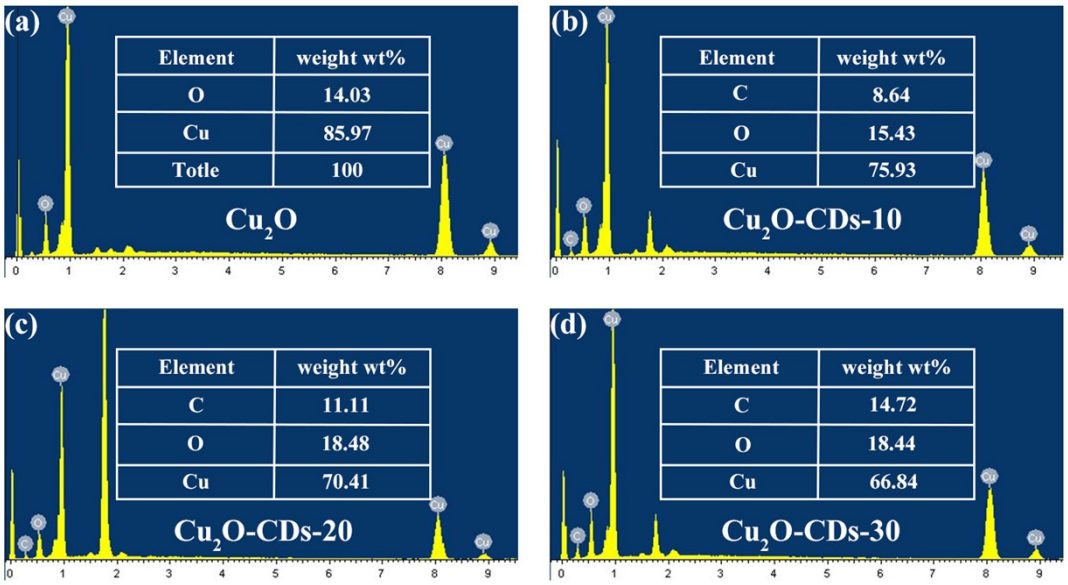

Figure S6. SEM-EDS of (a) pure Cu_2O, (b) Cu_2O-CDs-10, (c) Cu_2O-CDs-20 and (d) Cu_2O-CDs-30.

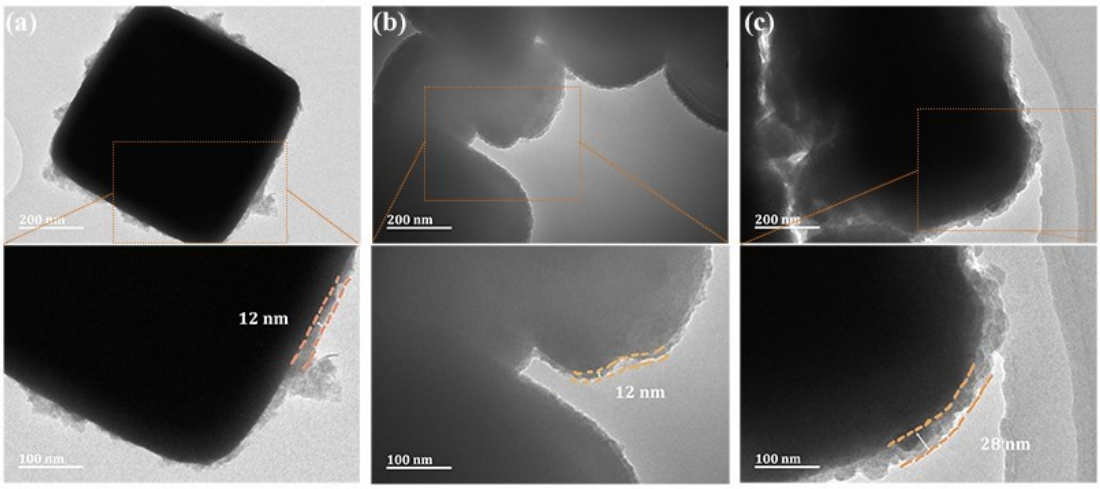

Figure S7. TEM images of (a) Cu_2O-CDs-10, (b) Cu_2O-CDs-20 and (c) Cu_2O-CDs-30.

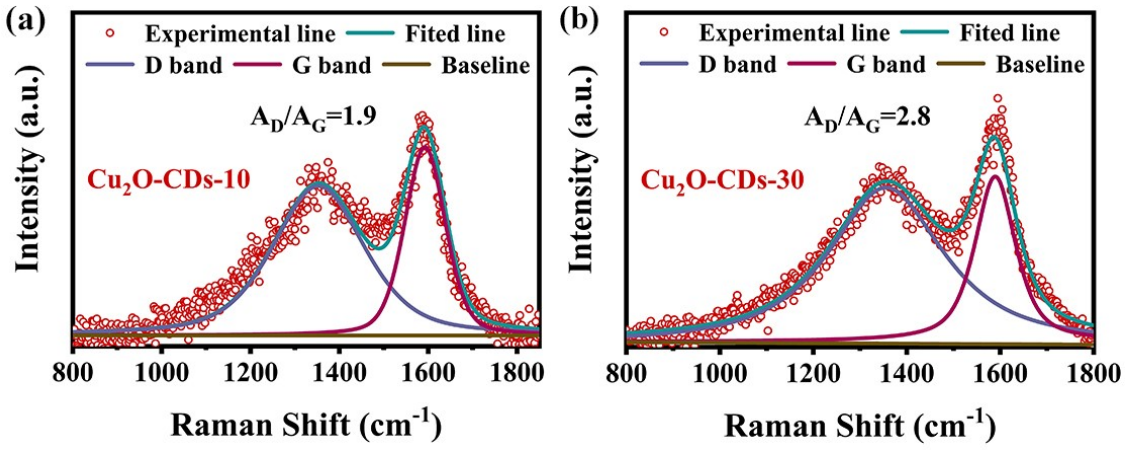

Figure S8. The fitted Raman patterns of (a) Cu_2O-CDs-10 and (b) Cu_2O-CDs-30.

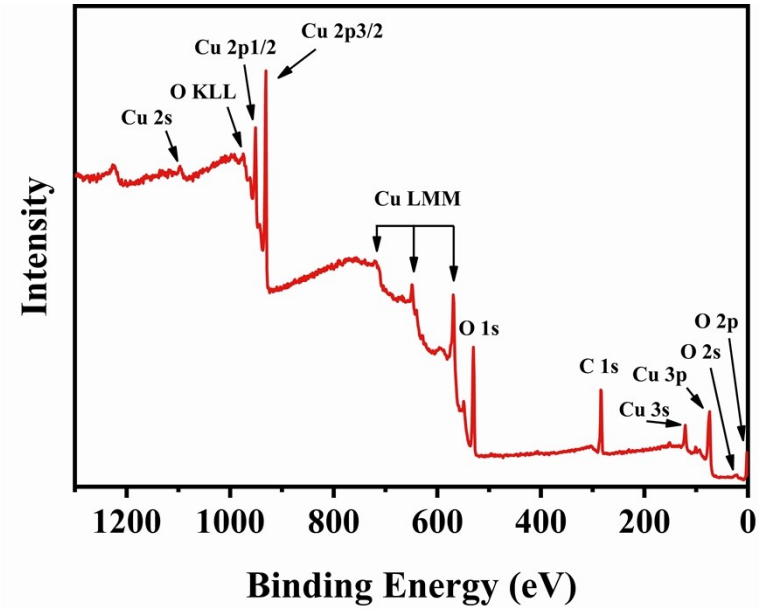

Figure S9. XPS-survey of Cu_2O-CDs-20.

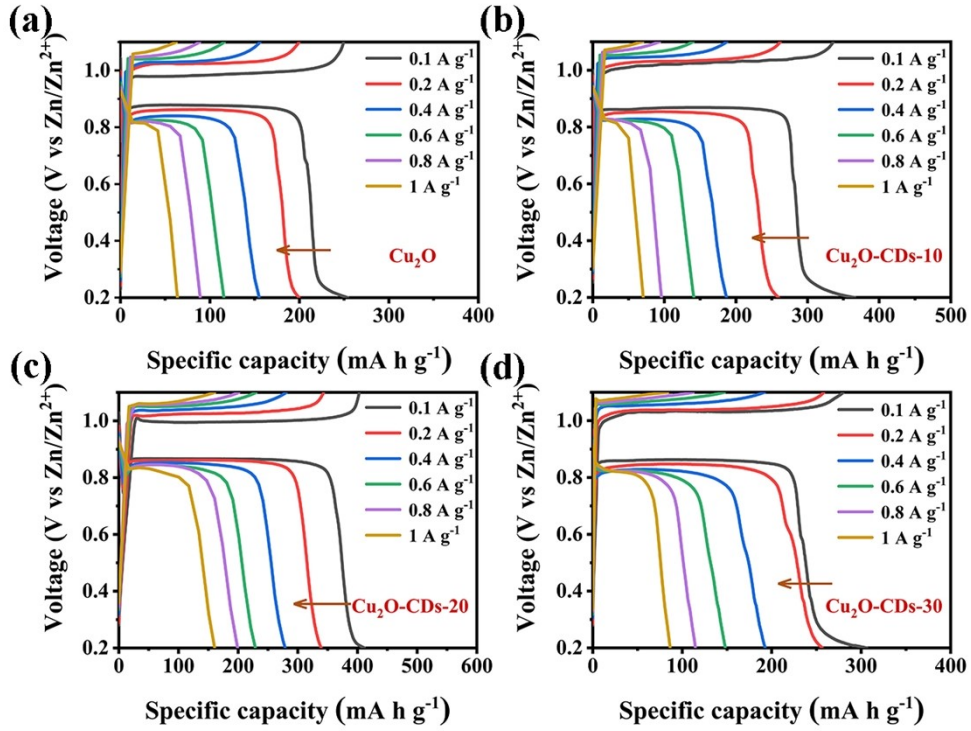

Figure S10. GCD curves of Cu_2O-CDs-X and Cu_2O electrodes at different current densities.

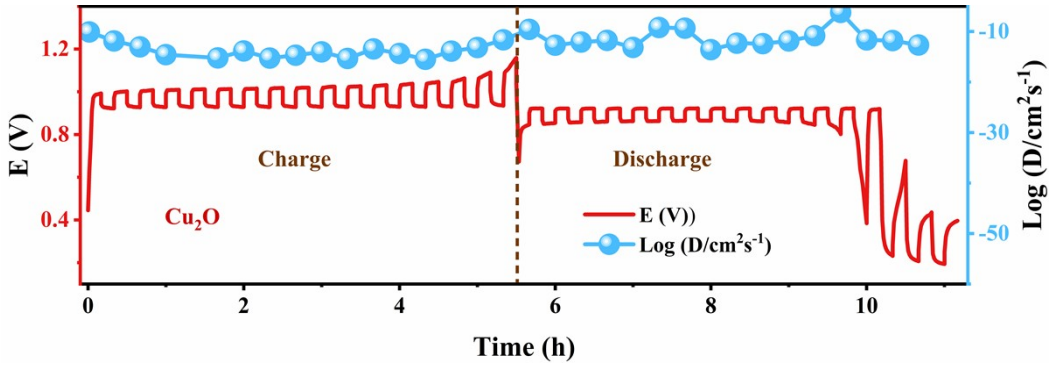

Figure S11. GITT profiles and the calculated Zn^{2+} diffusion $(D_{Zn^{2+}})$ values for the third cycle of Cu_2O electrode.

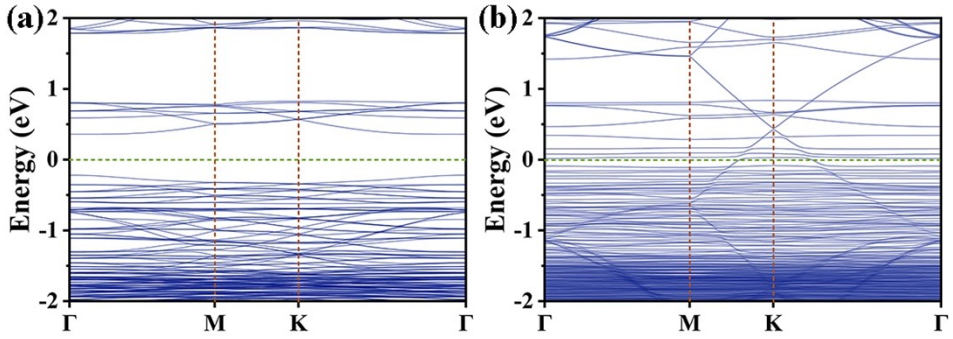

Figure S12. Energy band structures of (a) pure Cu_2O and (b) Cu_2O-CDs-20.

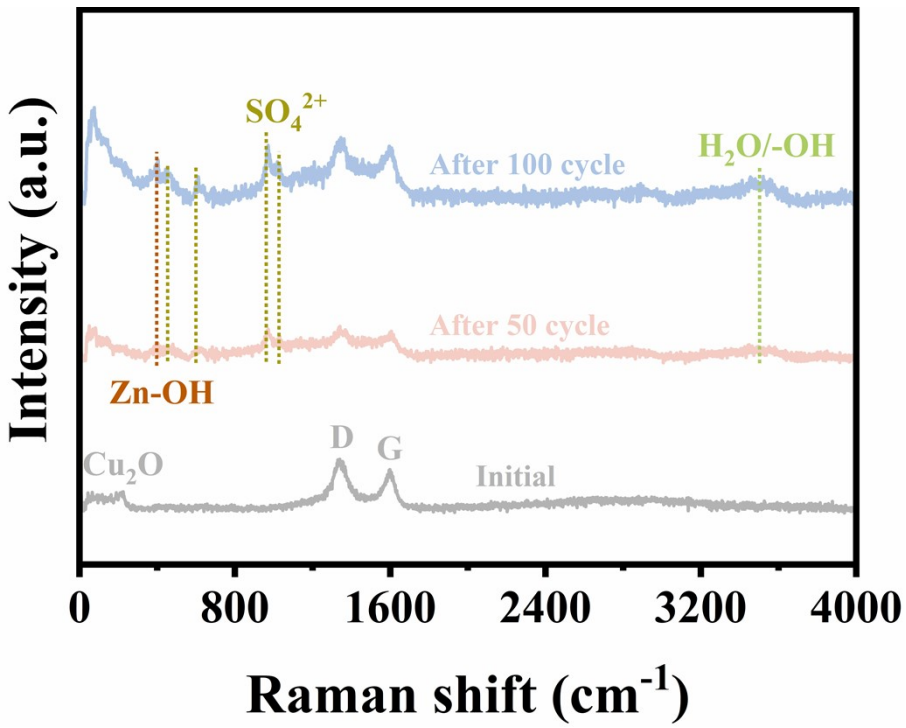

Figure S13. Raman spectra of Cu_2O-CDs-20 after different cycles.

Table S1. Crystal plane spacing obtained by XRD patterns

Simple	*d(110)*	*d(111)*	*d(200)*	*d(220)*	*d(311)*
Pure Cu_2O	3.0235	2.4669	2.1359	1.5097	1.287
Cu_2O -CDs-10	3.0275	2.4702	2.1383	1.5072	1.2874
Cu_2O -CDs-20	**3.0275**	**2.4702**	**2.1388**	**1.5108**	**1.2882**
Cu_2O -CDs-30	3.0235	2.4669	2.1359	1.5099	1.2873

Table S2. Parameters of equivalent circuit for all samples

Sample	R_s (Ω)	R_{ct} (Ω)	R_w (Ω)
Cu_2O	2.883	902.2	0.72
Cu_2O-CDs-10	2.914	480.6	0.60
Cu_2O-CDs-20	**2.815**	**306.2**	**0.54**
Cu_2O-CDs-30	3.373	119.9	0.56
Cu_2O-CDs-20 (after 1st)	4.863	391.0	0.60231
Cu_2O-CDs-20 (after 3rd)	6.81	863.1	0.31526

Table S3. Calculated adsorption energy of Zn^{2+} on the surface of Cu_2O-CDs-20 and Cu_2O

Simple	E_A (a.u.)	E_B (a.u.)	E_C (a.u.)	E_{ads} (eV)
Cu_2O-CDs-20 (Zn)	**-3103.64965**	**-3043.15368**	**-60.48693**	**-0.246**
Cu_2O (Zn)	-2754.73245	-2694.22582	-60.48693	-0.536

Table S4. Comparison of the electrochemical performance of Cu_2O-CDs-20 cathodes and previously reported Cu-based cathodes in AZIBs

cathodes	Electrolyte	Capacity	Current density	Reference
$Cu_{0.95}V_2O_5$	3 M $Zn(CH_3F_3SO_3)_2$	405 mA h g^{-1}	0.1A g^{-1}	R1
CuO	3 M $ZnSO_4$	230 mA h g^{-1}	0.1 A g^{-1}	R2
CuI	3 M $ZnSO_4$	105 mA h g^{-1}	0.1 A g^{-1}	R3
$Cu_{2-x}Te$	3 M $Zn(CH_3F_3SO_3)_2$	158 mA h g^{-1}	0.03 A g^{-1}	R4
CuSe	0.5 M $CuSO_4$ and 0.5 M $ZnSO_4$	346 mA h g^{-1}	0.5 A g^{-1}	R5
CuS_{1-x}@PANI	3 M $ZnSO_4$	198.5 mA h g^{-1}	0.1 A g^{-1}	R6
CuS@CTMAB	2 M $ZnSO_4$	287.5 mA h g^{-1}	0.2 A g^{-1}	R7
CuV_2O_6	3 M $Zn(CH_3F_3SO_3)_2$	427 mA h g^{-1}	0.1 A g^{-1}	R8
Cu_2O-CDs	**2 M $ZnSO_4$**	**425 mA h g^{-1}**	**0.1 A g^{-1}**	**This work**

Reference

[R1] Yu, X.; Hu, F.; Guo, Z. Q.; Liu, L.; Song, G. H.; Zhu, K. High-Performance Cu0.95V2O5 Nanoflowers as Cathode Materials for Aqueous Zinc-Ion Batteries. *Rare Metals* **2021**, *41* (1), 29-36.

[R2] Meng, J.; Yang, Z.; Chen, L.; Qin, H.; Cui, F.; Jiang, Y.; Zeng, X. Energy Storage Performance of CuO as a Cathode Material for Aqueous Zinc Ion Battery. *Mater. Today Energy* **2020**, *15*, 100370-100377.

[R3] Meng, J.; Yang, Z.; Chen, L.; Zeng, X.; Chen, H.; Cui, F.; Jiang, Y. The Investigation on the Electrochemical Performance of CuI as Cathode Material for Zinc Storage. *Electrochim. Acta* **2020**, *338*, 135915-135922.

[R4] Li, W.; Ma, Y.; Li, P.; Jing, X.; Jiang, K.; Wang, D. Electrochemically Activated $Cu_{2-x}Te$ as an Ultraflat Discharge Plateau, Low Reaction Potential, and Stable Anode Material for Aqueous Zn-Ion Half and Full Batteries. *Adv. Energy Mater.* **2021**, *11* (42), 2102607-2102618.

[R5] Wang, Y.; Wang, B.; Zhang, J.; Chao, D.; Ni, J.; Li, L. Conversion Electrochemistry of Copper Selenides for Robust and Energetic Aqueous Batteries. *Carbon Energy* **2022**, *5* (2), e261.

[R6] Lei, Q.; Zhang, J.; Liang, Z.; Yue, Y.; Ren, Z.; Sun, Y.; Yao, Z.; Li, J.; Zhao, Y.; Yin, Y.; et al. Synergistic Engineering of Sulfur Vacancies and Heterointerfaces in Copper Sulfide Anodes for Aqueous Zn-Ion Batteries with Fast Diffusion Kinetics and an Ultralong Lifespan. *Adv. Energy Mater.* **2022**, *12* (21), 2200547-2200557.

[R7] Lv, Z.; Wang, B.; Ye, M.; Zhang, Y.; Yang, Y.; Li, C. C. Activating the Stepwise

Intercalation-Conversion Reaction of Layered Copper Sulfide toward Extremely High Capacity Zinc-Metal-Free Anodes for Rocking-Chair Zinc-Ion Batteries. *ACS Appl. Mater. Interfaces* **2022**, *14* (1), 1126-1137.

[R8] Liu, Y.; Li, Q.; Ma, K.; Yang, G.; Wang, C. Graphene Oxide Wrapped CuV(2)O(6) Nanobelts as High-Capacity and Long-Life Cathode Materials of Aqueous Zinc-Ion Batteries. *ACS Nano* **2019**, *13* (10), 12081-12089.

Table of Contents Entry

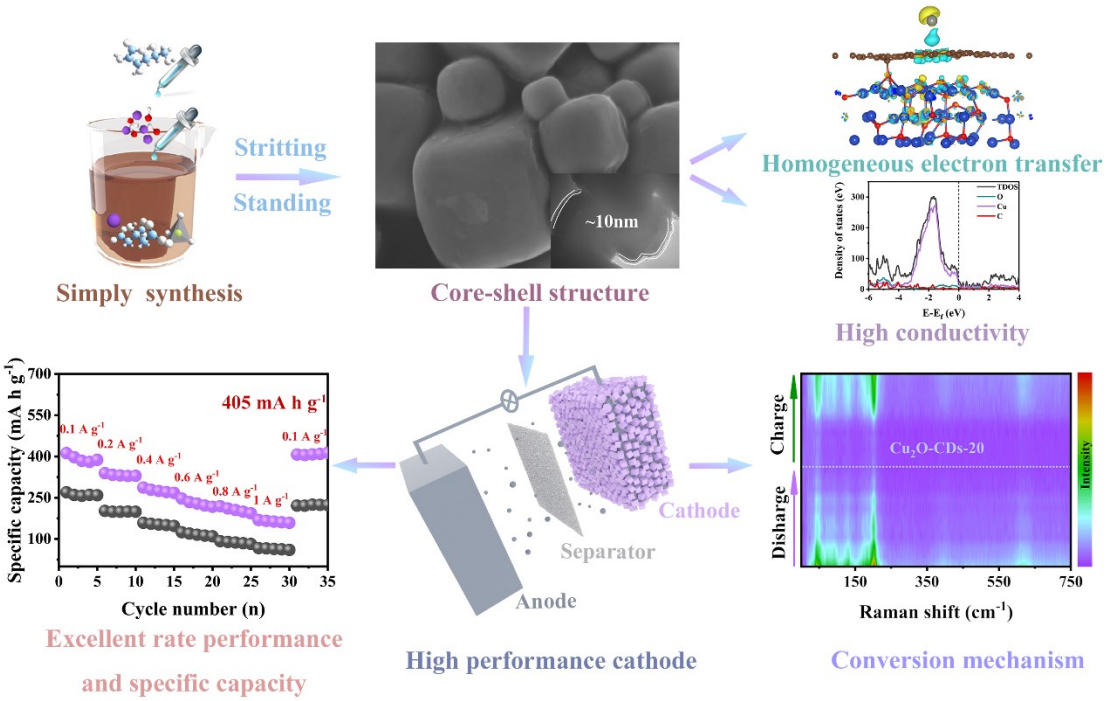

Core-shell structure of Cu_2O constructed by carbon quantum dots exhibited high discharge specific capacity and excellent rate performance. And the conversion-type zinc storage mechanism was confirmed by in-situ XRD and in-situ Raman technology.